

Direct observation of cooperative effects in capillary condensation: The hysteretic origin

Fèlix Casanova,^{a)} Casey E. Chiang, Chang-Peng Li, and Ivan K. Schuller
Physics Department, University of California-San Diego, La Jolla, California 92093, USA

(Received 3 October 2007; accepted 19 November 2007; published online 10 December 2007)

We tailor anodized alumina with pores with well-defined, simple geometries, in order to study the effects of constrictions in hysteretical capillary condensation, independently from other cooperative processes such as network effects. We confirm, by direct observation using optical interferometry, the occurrence of two cooperative phenomena: the classical pore blocking effect in nearly ideal “inkbottle” pores and the advanced adsorption in pores with a change in the cross section. They are relevant for the development of a theory of the poorly understood hysteresis in complex porous materials. © 2007 American Institute of Physics. [DOI: 10.1063/1.2822815]

Nanoporous materials have promising properties that can be used both in applications (biosensing,¹ chemical sensing,² nanotemplates,³...) and in fundamental studies, e.g., phase transitions in confined geometries.⁴ In particular, capillary condensation in nanopores has been studied in a wide variety of materials, comprised mostly of disordered/interconnected porous materials such as compacted powder, oxide xerogels or Vycor glass,⁵ but direct comparison with theoretical work has been difficult due to the lack of ideal geometries in the pores.^{6,7} Hysteresis in capillary condensation is a phenomenon that is still poorly understood, and is thus still an open issue.^{8,9}

The classical pore blocking effect in inkbottle-type pores⁵ has usually been employed to describe type H2 hysteresis loops in disordered/interconnected porous materials.^{10,11} Recent simulation^{12–15} and theoretical^{15,16} works in single pores with constrictions predict either pore blocking (the liquid can only evaporate when the constriction, which isolates the pore from the gas reservoir, empties) or cavitation (the liquid in the pore reaches its limit of stability while the constriction is still full and evaporation occurs via nucleation of a gas bubble) effects, depending on pore geometry and temperature. Experimental pore blocking and/or cavitation effects have been indirectly observed in ordered cagelike pore structures of SBA-16 (Refs. 17 and 18) and FDU-1 (Ref. 17) silicas. These porous silicas have been considered the best available models for inkbottle pore systems, although the pores are interconnected¹⁹ (and therefore network effects can also occur), and they may present intrawall pores (diameters <2 nm) as well as difficult synthesis reproducibility.^{19,20} Tailored inkbottle pores in silicon have also been used, but no pore blocking was observed.²¹ Another effect, advanced adsorption (the meniscus—liquid-vapor interface—created in a narrow pore section full of liquid propagates into a contiguous wider section) has also been used to explain adsorption in interconnected²² or undulating²³ pores, although it has only been observed indirectly.²³

Recently, capillary condensation has been observed in anodized nanoporous alumina,^{9,24} a suitable material which can be tailored by controlling anodization parameters.^{3,25} In this letter, we present alumina nanopores tailored with simple

geometries. With optical interferometry, one can independently monitor adsorption and desorption in every part of the pore, and thus directly observe the occurrence of pore blocking and advanced adsorption effects. These cooperative effects are important for the development of a theory for hysteresis in complex porous systems.²⁶

Nanoporous alumina double-layer samples were prepared by depositing a thick aluminum film (6–12 μm) by e-beam evaporation on a *n*-Si substrate.³ The periodicity of the pore arrays and the pore diameters were controlled by choice of both the electrolyte and anodization voltages. The top layer was obtained by a two-step anodization,²⁵ using 40 V and 0.3M oxalic acid for one sample (“funnel”) and 15 V and 2.6M sulfuric acid for the other (“inkbottle”). Subsequent acid etching for 55 min was used in the former sample to remove the barrier layer at the bottom of the pores³ so as to be able to anodize a second layer. We note that this process also widens the pores without affecting the periodicity. No etching was used in the inkbottle sample. The bottom layer was obtained by a one-step anodization using 19 V and 2.6M sulfuric acid for the funnel sample and 40 V and 0.3M oxalic acid for the inkbottle sample. Finally, acid etching for 5 min was performed in both samples. The pore geometry was determined from scanning electron microscopy (SEM) images (Fig. 1). Cross-sectional images show that the funnel sample presents a large cylindrical pore section (64±10 nm of diameter) at the top layer and a smaller one (15±3 nm) at the bottom, whereas the inkbottle sample presents a small cylindrical pore section (14±3 nm) at the top layer and a larger one (27±3 nm) at the bottom. The pores are thus funnel- or inkbottle shaped and without interconnections.

Reflectance spectra were obtained using a white light source and a spectrometer, based on a linear charge coupled device array, in a 90° backscattering configuration, as previously described.²⁴ The spectra display a complex series of fringes [Fig. 2(a)] which results from interference of the light beams reflected at the three interfaces of the porous alumina double layer [beams a, b, and c in the inset of Fig. 2(b)]. Since the pore diameters are much smaller than the light wavelength λ, each porous layer acts as a single medium with an average refractive index *n*. For a single layer, the fringe maxima are described by the relationship $m\lambda = 2nL$, where *m* is an integer and *L* is the thickness of the layer. The term $2nL$ is the effective optical thickness of the layer. Fill-

^{a)}Electronic mail: casanova@physics.ucsd.edu.

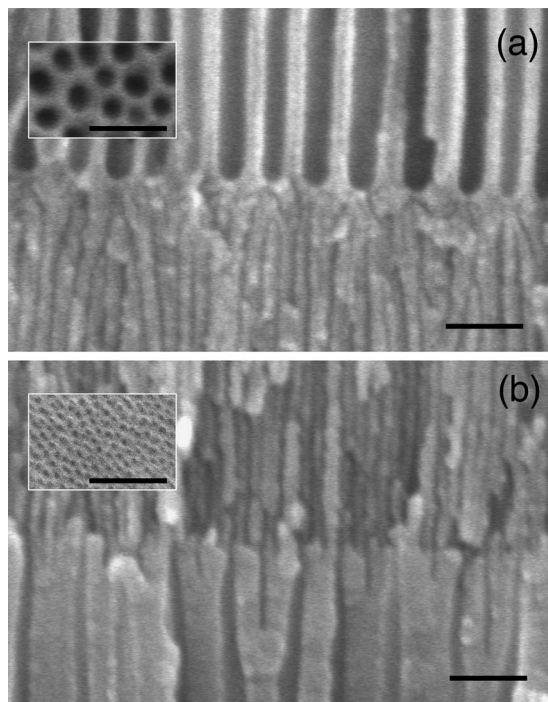


FIG. 1. Cross-sectional SEM images of alumina double-layer samples: (a) “Funnel” sample with 64 ± 10 nm pore diameter at top and 15 ± 3 nm pore diameter at the bottom and (b) “inkbottle” sample with 14 ± 3 nm pore diameter at top and 27 ± 3 nm pore diameter at the bottom. Insets: top-view SEM images of the corresponding samples. Scale bars are 200 nm.

ing the pores with an analyte results in a change of n , thus shifting the fringes. The value of $2nL$ can be obtained directly as the position of the peak in the fast Fourier transform (FFT) of the reflectance spectrum, which can be resolved down to ~ 1 nm. If the film has a double layer, as in our case, the FFT yields values of $2nL$ for each layer as distinct peaks [see Fig. 2(b)]. The sum of the values of $2nL$ for layers 1 and 2 is predicted to be equal to the value for layer 3 (Ref. 1).

Gas dosing was performed in a Teflon cell fitted with a glass window. Saturated vapor analyte was generated by bubbling pure N_2 through the liquid analyte at $25^\circ C$ and then diluted by mixing the effluent with pure N_2 using a computer-controlled gas dosing system. Relative vapor pressures, P/P_s , where P_s is the saturation vapor pressure, were calculated using the dilution ratio of the gas dosing system. All samples were dosed with hexane, isopropanol, and tolu-

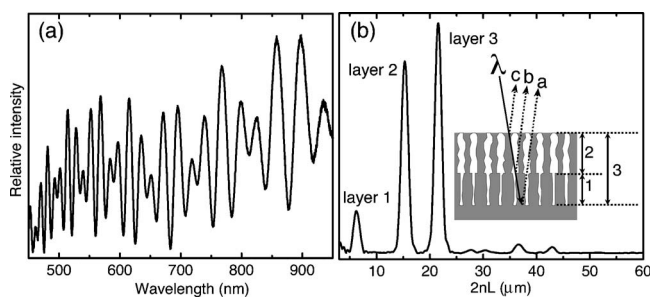


FIG. 2. (a) Reflectance spectrum of alumina double-layer funnel sample. (b) FFT of the spectrum, showing the peaks corresponding to the effective optical thickness ($2nL$) of each layer. Inset in (b): schematic of the double-layer sample showing the three different interfering optical paths. Interference of beams a and b occurs from reflections at the interfaces bordering layer 1, interference of beams b and c originates from layer 2, and interference of beams a and c originates from layer 3.

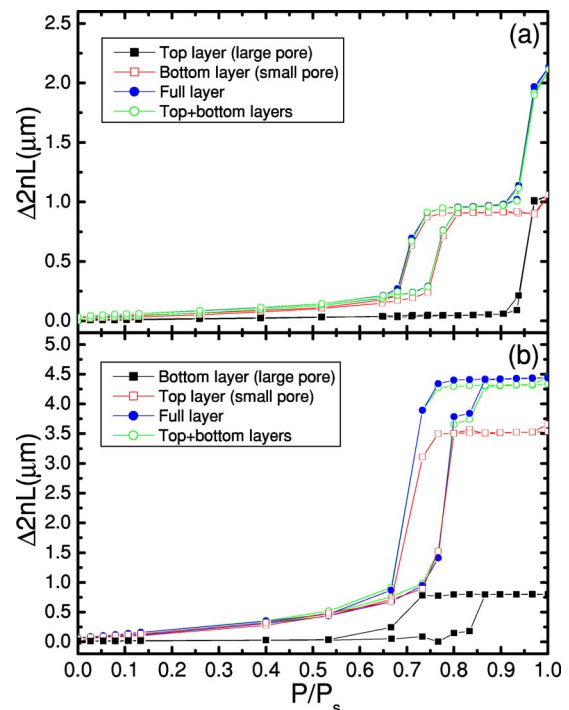


FIG. 3. (Color online) Change in $2nL$ as a function of the relative pressure of hexane in the (a) funnel and (b) inkbottle samples. Isotherms were obtained by first increasing (adsorption) and then decreasing (desorption) the relative pressure in discrete steps. Solid (empty) squares correspond to the adsorption isotherm of the single layer with larger (smaller) pore diameter, solid circles correspond to the full double-layer and empty circles are the sum of the two single layers. The size of the error bars is smaller than the size of the symbols.

ene. The three values of $2nL$ were simultaneously monitored while P/P_s was increased and subsequently decreased stepwise. For each step, the change in $2nL$ [$\Delta(2nL)$] with respect to the baseline obtained in pure N_2 , i.e., with empty pores, was plotted as a function of P/P_s . Since $\Delta(2nL)$ is uniquely related to the volume of analyte adsorbed into the pores, this directly provides the adsorption-desorption isotherms.⁵ Every isotherm was repeated up to seven times to check reproducibility. Therefore, with this interferometric technique, we can monitor independently the adsorption process of every part of the pore.

The isotherms exhibited by each sample show a complex shape, the same for all three analytes (see solid circles in Fig. 3 for hexane). These are very different from those obtained in simple alumina nanopores,²⁴ which are type IV and display a single type H1 hysteresis loop.¹¹ However, if one looks at the adsorption-desorption isotherms for each part of the pore, the entire process can be easily understood. In general, the capillary behavior can be described by the Kelvin equation,⁵ which for cylindrical pores with a hemispherical meniscus takes the form

$$\ln\left(\frac{P}{P_s}\right) = -\frac{2\gamma V_L}{RT r_m}, \quad (1)$$

where r_m is the radius of the meniscus, R is the ideal gas constant, and V_L and γ are the molar volume and surface tension of the liquid at temperature T . According to theoretical approaches,^{6,7} Eq. (1) is valid for pore diameters ≥ 7.5 – 10 nm, and has been experimentally verified in cylindrical pores with diameters ≥ 10 nm.²⁴

In the funnel sample [Fig. 3(a) for hexane], capillary condensation (steep increase in the isotherm slope) occurs first at the bottom layer (smaller pore diameter) upon adsorption. At higher P/P_S , a second condensation takes place, now at the top layer (larger pore diameter). On desorption, evaporation occurs first at the top layer, without hysteresis. At lower P/P_S , evaporation at the smaller pores occurs, in this case with hysteresis. Note that the sum of the isotherms for the top and the bottom layers is equal to the isotherm for the full layer, as expected. According to these results, adsorption in the small pores, i.e., at the bottom layer, proceeds as if corresponding to a single pore: condensation occurs by nucleation in metastable states, but evaporation occurs at the true equilibrium transition because once the meniscus is formed after condensation, it can retreat on desorption.^{6,21,24} In the latter case, we can apply Eq. (1), which gives us a pore diameter of 12 nm, in agreement with SEM images. However, condensation and evaporation in the larger pores at the top layer both occur at the equilibrium P/P_S , since this value corresponds to a pore diameter of 59 nm when using Eq. (1), in agreement with SEM images. This fact shows that the menisci, formed at the bottom layer after the condensation of the small pores, advance into the larger pores when P/P_S is increased up to the equilibrium value of the large pores, thus avoiding the metastable nucleation from the pore walls as observed for single pores. This long-predicted phenomenon, advanced adsorption,^{22,23} has never been observed directly before.

In the inkbottle sample [Fig. 3(b) for hexane], capillary condensation also occurs first within the smaller pores on adsorption, in this case at the top layer. At higher P/P_S , the second condensation at the larger pores (bottom layer) occurs. On desorption, however, evaporation takes place at both layers almost at the same pressure, giving rise to hysteresis in both layers. The sum of the isotherms for the top and the bottom layers is again equal to the isotherm for the full layer. According to these results, condensation at the smaller pores at the top takes place from a metastable state. At higher P/P_S , when the equilibrium transition for the larger pores at the bottom is reached, the menisci at the lower part of the small pores propagate into the large pores by diffusion of the fluid from the external gas reservoir,^{12,18,22} avoiding the metastable nucleation (i.e., advanced adsorption takes place again). Equation (1) yields a pore diameter of 27 nm for the large pores, in agreement with SEM images. A detailed examination at the pressures for all isotherms (different runs and analytes) shows that evaporation occurs first at the small pores and, after it empties, the large pores start evaporating. P/P_S values correspond to a pore diameter of 13 nm [Eq. (1)], demonstrating that equilibrium evaporation at the small pores controls evaporation from the large pores. Indeed, we are directly observing the classical pore blocking effect in inkbottle-type pores. This is in contrast with results in tailored porous silicon,²¹ where the nonuniformity of the pores and not the inkbottle geometry controls capillary hysteresis. A better pore geometry (independent, cylindrical

pores with narrow diameter distribution and regular section) in alumina²⁴ can explain this difference.

To conclude, anodized alumina can be tailored with independent pores with simple (inkbottle and funnel) geometries in order to study the effect of pore morphology in capillary condensation, independently from network effects. We confirm, by using optical interferometry, the occurrence of two cooperative phenomena: the classical pore blocking effect in nearly ideal inkbottle pores and advanced adsorption in pores with a change in the cross section, both of which have been predicted in theoretical and simulation works, but not directly observed experimentally before. This will help in the development of a theory of the poorly understood hysteresis in disordered/interconnected porous materials.

We thank Professor M. J. Sailor for his help with optical interferometry. The financial support of the AFOSR is acknowledged. F.C. acknowledges financial support from Spanish MEC and Fulbright Commission.

¹C. Pacholski, M. Sartor, M. J. Sailor, F. Cunin, and G. M. Miskelly, *J. Am. Chem. Soc.* **127**, 11636 (2005).

²J. Gao, T. Gao, Y. Y. Li, and M. J. Sailor, *Langmuir* **18**, 2229 (2002).

³C. Li, I. V. Roshchin, X. Batlle, M. Viret, F. Ott, and I. K. Schuller, *J. Appl. Phys.* **100**, 074318 (2006).

⁴L. D. Gelb, K. E. Gubbins, R. Radhakrishnan, and M. Sliwinski-Bartkowiak, *Rep. Prog. Phys.* **62**, 1573 (1999).

⁵S. J. Gregg and K. S. W. Sing, *Adsorption, Surface Area and Porosity* (Academic, London, 1982), pp. 111–194.

⁶A. V. Neimark, P. I. Ravikovitch, and A. Vishnyakov, *Phys. Rev. E* **62**, R1493 (2000).

⁷M. Kruk, M. Jaroniec, and A. Sayari, *Langmuir* **13**, 6267 (1997).

⁸R. Valiullin, S. Naumov, P. Galvosas, J. Kärger, H.-J. Woo, F. Porcheron, and P. A. Monson, *Nature (London)* **443**, 965 (2006).

⁹K. J. Alvine, O. G. Shpyrko, P. S. Pershan, K. Shin, and T. P. Russell, *Phys. Rev. Lett.* **97**, 175503 (2006).

¹⁰D. H. Everett, in *The Solid-Gas Interface*, edited by E. A. Flood (Dekker, New York, 1967), Vol. 2, pp. 1055–1113.

¹¹K. S. W. Sing, D. H. Everett, R. A. W. Haul, L. Moscou, R. A. Pierotti, J. Rouquérol, and T. Siemieniewska, *Pure Appl. Chem.* **57**, 603 (1985).

¹²L. Sarkisov and P. A. Monson, *Langmuir* **17**, 7600 (2001).

¹³A. Vishnyakov and A. V. Neimark, *Langmuir* **19**, 3240 (2003).

¹⁴B. Coasne and R. J. Pellenq, *J. Chem. Phys.* **121**, 3767 (2004).

¹⁵B. Libby and P. A. Monson, *Langmuir* **20**, 4289 (2004).

¹⁶P. I. Ravikovitch and A. V. Neimark, *Langmuir* **18**, 1550 (2002a).

¹⁷P. I. Ravikovitch and A. V. Neimark, *Langmuir* **18**, 9830 (2002b).

¹⁸K. Morishige and M. Tateishi, *J. Chem. Phys.* **119**, 2301 (2003).

¹⁹Y. Sakamoto, M. Kaneda, O. Terasaki, D. Y. Zhao, J. M. Kim, G. Stucky, H. J. Shin, and R. Ryoo, *Nature (London)* **408**, 449 (2000).

²⁰P. Van Der Voort, M. Benjelloun, and E. F. Vansant, *J. Phys. Chem. B* **106**, 9027 (2002).

²¹D. Wallacher, N. Kovalev, N. Knorr, and K. Knorr, *Phys. Rev. Lett.* **92**, 195704 (2004).

²²V. Mayagoitia, F. Rojas, and I. Kornhauser, *J. Chem. Soc., Faraday Trans. 1* **81**, 2931 (1985).

²³J. M. Esparza, M. L. Ojeda, A. Campero, A. Domínguez, I. Kornhauser, F. Rojas, A. M. Vidales, R. H. López, and G. Zgrablich, *Colloids Surf., A* **241**, 35 (2004).

²⁴F. Casanova, C. E. Chiang, C. Li, I. V. Roshchin, A. M. Ruminski, M. J. Sailor, and I. K. Schuller, *Europhys. Lett.* (in press).

²⁵H. Masuda and K. Fukuda, *Science* **268**, 1466 (1995).

²⁶B. Coasne, K. E. Gubbins, and R. J.-M. Pellenq, *Phys. Rev. B* **72**, 024304 (2005).